

Improving the H.E.S.S. angular resolution using the Disp method

CHIA-CHUN LU¹ FOR THE H.E.S.S. COLLABORATION.

¹ Max-Planck-Institut fuer Kernphysik, Saupfercheckweg 1, 69117 Heidelberg, Germany

c.lu@mpi-hd.mpg.de

Abstract: The angular resolution of imaging atmospheric Cherenkov telescopes depends on the employed event reconstruction methods. By taking the weighted average of intersections of shower axes, the H.E.S.S. experiment achieves a 0.08 degree angular resolution at 20 degree zenith angle with an image size cut of 160 p.e. for sources with a spectral index of 2. However, the angular resolution degrades to 0.14 degree at 60 degree zenith angle, due to the larger fraction of nearly parallel images. The Disp method reduces the impact of parallel images by including an estimation of the image displacement (disp), inferred from the Hillas parameters, in the reconstruction procedure. By using this technique, the angular resolution at large zenith angles can be improved by 50%. An additional cut on the estimated direction uncertainty can further improve the angular resolution to around 0.05 degrees at the expense of a loss of 50% of effective area. The performance of this reconstruction method on simulated γ -ray events and real data is presented.

Keywords: direction reconstruction, gamma-ray astronomy

1 Introduction

The imaging atmospheric Čerenkov telescopes (IACT) technique has been developed for several decades. IACTs detect the Čerenkov light emitted by relativistic charged particles in atmospheric air showers induced by very-high-energy (\sim TeV) γ rays. The Čerenkov light distribution is imaged onto the cameras. Stereoscopic observation of air showers with IACT arrays has been proven successful in providing better direction reconstruction and background rejection. The quality of direction reconstruction can be quantified by the 68% containment radius, R_{68} , of the point-spread function which is also referred to as the angular resolution. For γ -ray sources with a given spectrum, the angular resolution depends on the design of the instruments, the analysis cuts, and the event reconstruction algorithm. As discussed in [1], the reconstruction algorithms mainly follow two approaches. The first kind is based on parameterizing the image as an ellipse, characterized by the first and second moments of image intensity distribution (the so-called *Hillas parameters* [2]), and the second kind is based on a global fit to pixel amplitudes.

In the analysis, the raw data is first calibrated. In the Hillas-type approach, the pixel noise produced mainly by night sky background photon is reduced by image cleaning before image parameterization. The total image intensity is denoted as *size* and the center of gravity of pixel intensity distribution (the first moment) is *c.o.g.* (see Figure 1). The second moments of the *Hillas ellipse* are the *length* and *width*. The orientation of major axis with respect to the x-axis of the coordinate system is defined as ϕ . The event direction can be calculated by *Algorithm 1* in [1] using the pair-wise intersections of extended major axes averaged by weighting factors, composed of combinations of *Hillas parameters*.

The drawback of this method is that the angular resolution degrades rapidly at larger zenith angles where the *impact parameters*, defined as the perpendicular distance between the shower axis and the telescope, get on average larger. The images of showers at larger distances from the

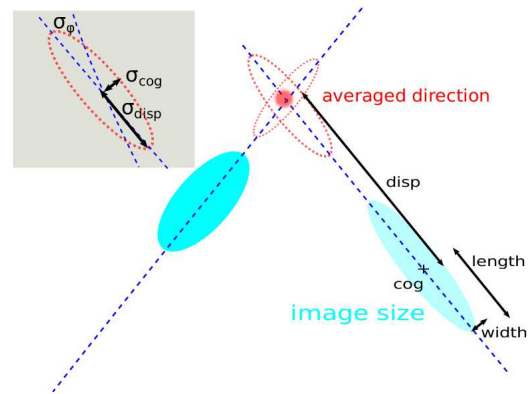


Fig. 1: Schematic diagram representing the *Hillas parameters* and *image parameters*. The working principle of the *Disp method* (*Algorithm 3*) is illustrated. The definition of σ_{disp} , σ_{cog} , and σ_{ϕ} are displayed in the grey box.

telescopes are more elongated. The axes of different images get more parallel than those of showers at smaller distances. This reflects the smaller difference in the viewing angles of different telescopes. The advantages of stereoscopic observation are thus reduced.

2 Method

Event reconstruction can be improved by introducing additional *image parameters*. The *disp*, defined as the angular distance between *c.o.g.* and event direction, the uncertainties of *disp*, *c.o.g.* and ϕ : σ_{disp} , σ_{cog} , and σ_{ϕ} . The prototype of this reconstruction method is referred to as *Algorithm 3* in [1], also called the *Disp method*, and used in IACT experiments such as HEGRA [1] and VERITAS [3] for stereoscopic reconstruction. The *image parameters* can be calculated by experiential formulae or lookup tables. In this work, multi-dimensional lookup tables filled with Monte-Carlo simulated γ -ray events are used. The lookup

Output	Parameters	X-axis	Y-axis
disp	opt,azm,zen,imp	ln(size/p.e.)	length
σ_{disp}	opt,azm,zen,imp	ln(size/p.e.)	length
σ_{cog}	opt,azm,zen	ln(size/p.e.)	width
σ_{ϕ}	opt,azm,zen	ln(size/p.e.)	width/length
imp'	opt,azm,zen	disp _{true}	\hat{H}_{max}

Table 1: The layout of the image parameter (output) lookup tables used in the *Disp method*. Here opt, azm, and zen are the abbreviation of telescope optical efficiency, azimuth and zenith angle of the event. The *disp* and σ_{disp} lookup tables have one extra parameter, *imp*, which is the *impact parameter* reconstructed by *Algorithm 1*. *Imp'* is used to reconstruct the new *impact position*. \hat{H}_{max} is the ratio of *impact parameter* over *disp* reconstructed by *Algorithm 1*.

tables are two-dimensional histograms stored as a function of azimuth angle, zenith angle, *impact parameter*, and optical collection efficiency. The layouts of the lookup tables are presented in Table 1. All parameters except the optical efficiency are pre-determined by using *Algorithm 1* before used in *Algorithm 3* to look up the values of *image parameters*. The *disp* lookup tables have one extra parameter, the *impact parameter*, to cope with the effect of image truncation due to the fixed 16ns read-out window of the H.E.S.S. cameras. When the spread of arrival times of photons emitted in the shower on the focal plane of a camera is larger than 16ns, the part of the shower beyond the read-out window is not recorded. This effect results in a reduced *length* and *image size* of the recorded shower image. The truncation usually happens for images of energetic showers with larger *impact parameters* whose longitudinal development is more extended in time.

For each image of an event, the *disp* and the orientation of the major axis yields an estimated event direction associated with an error ellipse, derived from the combination of σ_{disp} , σ_{cog} , σ_{ϕ} and represented by a covariance matrix. The averaged event direction is calculated by averaging telescope-wise event directions, weighted by the inverse of the determinant of the corresponding covariance matrix. The square root of the quadratic sum of the eigenvalues of the covariance matrix associated with the final event direction is an estimate of the uncertainty on the event direction. The *impact position*, which is defined as the intersection of the shower axis and the ground, is reconstructed in a similar way using *impact parameters* calculated from the lookup tables. The *impact parameter* is in the first order proportional to the product of *disp* and the height of shower maximum which are pre-estimated by *Algorithm 1* before used to look up the new *impact parameter* used in *Algorithm 3*.

3 Performance

3.1 Simulated γ -ray sources

The performance of this reconstruction method is tested with Monte-Carlo simulated γ -ray point sources under different observation conditions, e.g. different zenith angles and offset angles between the pointing direction and source direction. As shown in Figure 2, R_{68} is dependent on the spectral index of sources. Sources with softer spectra have in general poorer angular resolutions.

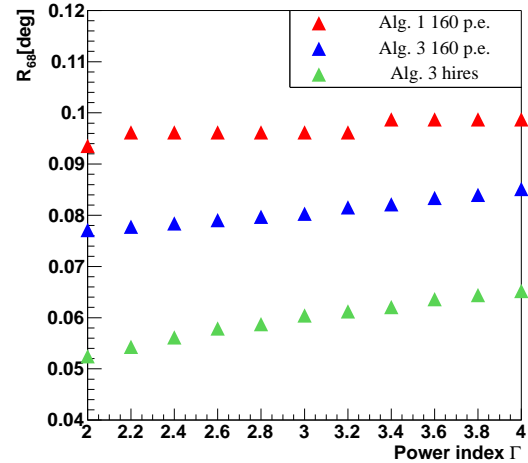


Fig. 2: Angular resolution (R_{68}) as a function of source spectral index at 45° zenith angle and 0.5° offset angle for *Algorithm 1* and *Algorithm 3*. The angular resolution is calculated with γ -ray spectra following a power law of a spectral index Γ . The events are reconstructed with images selected with *image size* larger than 160 p.e.. The *hires* configuration has an additional cut on direction uncertainty.

R_{68} of *Algorithm 1* and 3 as a function of zenith and offset angles is presented in Figure 3. The γ -ray energy distribution is assumed following a power law with a spectral index of 2. One can see that R_{68} of *Algorithm 3* degrades more slowly with increasing zenith and offset angles than that of *Algorithm 1*. For an offset of 2.5° , the R_{68} is significantly improved by *Algorithm 3* because of the increased fraction of showers at large distances from the telescopes.

Figures 5 and 6 shows the change of effective area by using *Algorithm 3*. Mainly two factors contribute to the change: The changes of the angular resolution and of the γ -hadron separation cut. At 60° zenith angle, the effective area is significantly increased due to the much better angular resolution. By introducing an extra cut of 0.08° on the direction uncertainty, R_{68} can be reduced to $\sim 0.05^\circ$ as shown in Figure 4 at the expense of a loss of $\sim 50\%$ of effective area. The effective area of low energy γ -rays by this so-called *hires* configuration is significantly reduced as shown in Figures 5 and 6 so it is more suitable for the analysis of sources with hard spectra.

3.2 Real data

Two well known point-like sources are used to compare the performance of the two presented methods: Mkn 421 and the Crab nebula. Mkn 421 is a bright BL Lac object at a redshift of $z = 0.031$ and was reported as a VHE γ -ray source in [5]. The Crab nebula is a young pulsar wind nebula at a distance of 2kpc. Given its high and steady flux at energies above 100 GeV, the Crab nebula is commonly used as a standard candle for VHE γ -ray telescopes. The H.E.S.S. detection of the Crab nebula was published in [4]. Both these two sources have a spectrum with spectral index softer than 2 and a cutoff at high energy.

The analysis of the two objects presented here is performed using the H.E.S.S. analysis software *hap* with direction reconstruction following *Algorithm 1* and 3. A fraction of the data used in the original publication is used, re-

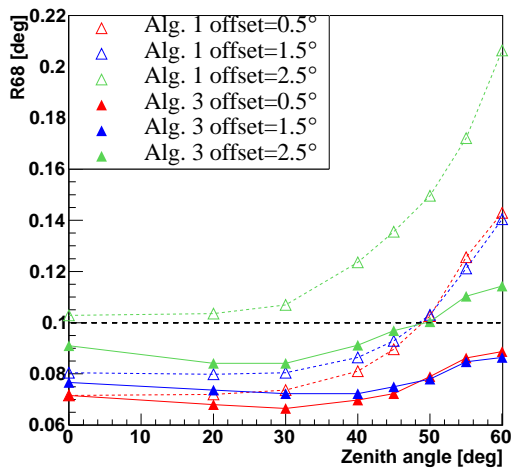


Fig. 3: Angular resolution (R_{68}) as a function of zenith angle at different offsets for *Algorithm 1* and *Algorithm 3*. The events are reconstructed with images selected with *image size* larger than 160 p.e.. The dashed line denotes the radius of the integration region used for deriving the source statistics listed in Table 2.

sulting in a mean observation zenith angle of 61° for Mkn 421 and 47° for the Crab nebula. γ -like events are selected following a Multivariate Analysis technique [6]. In this technique, parameters derived from image shapes and reconstructed physical quantities of the shower such as the depth of shower maximum and the sample standard deviation of the energies reconstructed by participating telescopes are used to reject the background-like events.

The statistics of γ -like events are summarized in Table 2. The *ring background* method is used to derive these quantities following the procedure described in [4]. Due to the stricter γ -hadron separation cut, the significance of Crab nebula is not changed much although the R_{68} is improved by using *Algorithm 3*.¹ The significance of Mkn 421 is significantly increased due to larger excess of γ -like events from the direction of the target. The squared angular distributions of γ -like excess events are presented in Figures 7 and 8. The distribution of Mkn 421 using *Algorithm 3* has a more pronounced peak around the target position and a shorter tail compared with that by *Algorithm 1*. The distribution of the Crab nebula by the *hires* cut has a $\sim 17\%$ smaller R_{68} and also a shorter tail compared with that by *Algorithm 3* with the 160-p.e size cut. The cut on the direction uncertainty reduces the number of γ -like events by $\sim 50\%$ but rejects even more hadronic events so the detection significance of point-like sources is kept $\sim 80\%$ as good as the configuration without this cut.

4 Conclusions

In this work, the performance of the direction reconstruction technique using the *Disp method* (*Algorithm 3*) is presented and compared with that of *Algorithm 1*. The angular resolution by *Algorithm 1* degrades rapidly with the zenith angle and is significantly improved by the *Disp method* at zenith angles larger than 45° . For events from large zenith angles of between 45° and 60° at 0.5° to 1.5° offsets, the improvement is $20\% - 40\%$. For offsets larger than 2.0° ,

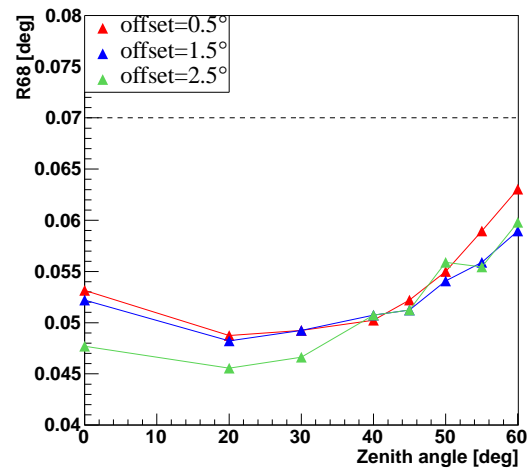


Fig. 4: Angular resolution (R_{68}) as a function of zenith angle at different offsets for the *hires* configuration. The events are reconstructed with images selected with *image size* larger than 160 p.e.. An extra cut on direction uncertainty of smaller than 0.08° is applied after reconstruction. The dashed line denotes the radius of the integration region used for deriving the source statistics listed in Table 2.

there is an additional improvement of $5\% - 10\%$. The *hires* configuration with an extra cut on the direction uncertainty achieves an angular resolution of $\sim 0.05^\circ$ at the expense of a loss of 50% of effective area.

This reconstruction technique can be applied widely to various kinds of sources taking the advantages of better angular resolution. The *hires* configuration with a significantly improved angular resolution is especially suitable for studies of sources with complicated morphology but high event statistics.

Acknowledgment: Please see standard acknowledgement in H.E.S.S. papers, not reproduced here due to lack of space.

References

- [1] W. Hofmann *et al.*, *Astroparticle Physics* 12 (1999) 135-143 doi:10.1016/S0927-6505(99)00084-5
- [2] A. M. Hillas, *Proceedings of the 19th International Cosmic Ray Conference* (1985) 445-448
- [3] G. D. Senturk, *Proceedings of the 32nd International Cosmic Ray Conference* (2011) 126-128
- [4] F. Aharonian *et al.*, *Astronomy and Astrophysics* 457 (2006) 899-915 doi:10.1051/0004-6361:20065351
- [5] F. Aharonian *et al.*, *Astronomy and Astrophysics* 437 (2005) 95-99 doi:10.1051/0004-6361:20053050
- [6] S. Ohm *et al.*, *Astroparticle Physics* 31 (2009) 383-391 doi:10.1016/j.astropartphys.2009.04.001
- [7] T.-P. Li and Y.-Q. Ma, *Astrophysical Journal* 272 (1983) 317-324 doi:10.1086/161295

1. The analysis cuts presented here are optimized for sources with a spectral index of 2 and 1% Crab flux.

Target	Config.	N_{On}	$N_{\text{Off}} \cdot \alpha$	Excess	Sig. [σ]	R_{68} [deg]
Mkn 421	Alg. 1	884	50	834	54	0.151
Mkn 421	Alg. 3	914	23	891	63	0.092
Mkn 421	hires	506	4	502	57	0.085
Crab	Alg. 1	1175	32	1143	70	0.094
Crab	Alg. 3	1056	21	1035	69	0.080
Crab	hires	548	4	544	58	0.070

Table 2: Statistics of γ -ray-like events from Mkn 421 and the Crab nebula. The image size cut is 160 p.e.. N_{On} is the event count within a circular integration region of the radius optimized for point-like source extraction which is 0.07° for the hires configuration and 0.1° for other configurations. $N_{\text{Off}} \cdot \alpha$ is the normalized background count. The excess is given as $N_{\text{On}} - \alpha N_{\text{Off}}$ and the significance (Sig.) is calculated following the formula 17 in [7].

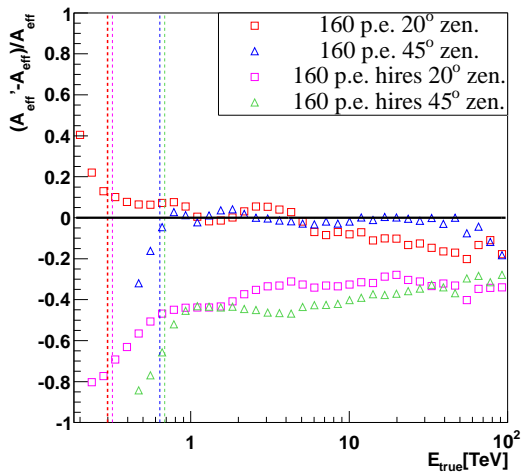


Fig. 5: Relative difference in effective area as a function of energy at 20° and 45° zenith angles. A'_{eff} : Effective area obtained by using *Algorithm 3*. A_{eff} : By using *Algorithm 1*. Dashed lines denote the safe energy threshold above which the energy bias is smaller than 10%.

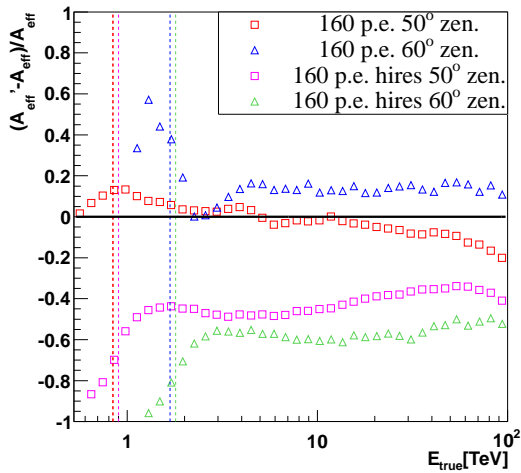


Fig. 6: Relative difference in effective area as a function of energy at 50° and 60° zenith angles.

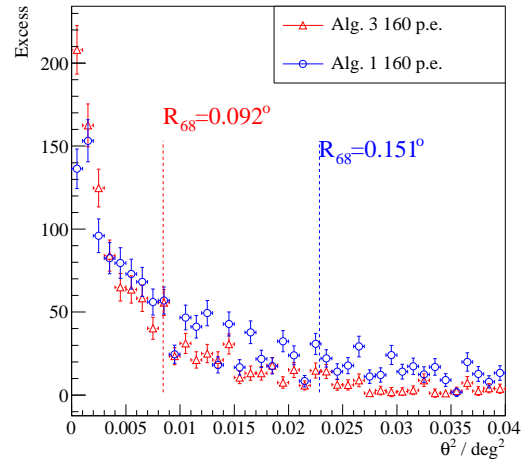


Fig. 7: Squared angular (θ^2) distribution of the excess events for Mkn 421. R_{68}^2 is denoted by the dashed line. The angular distance is calculated with respect to the position of Mkn 421.

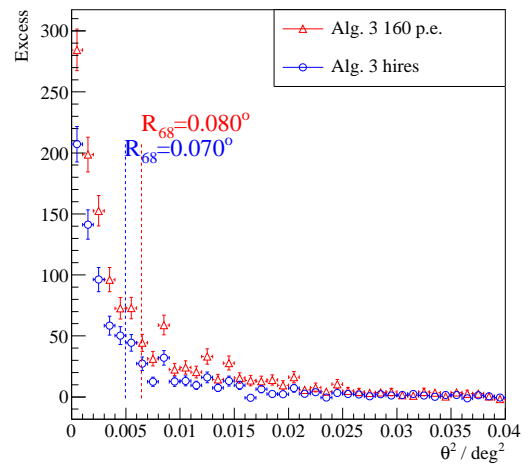


Fig. 8: Squared angular (θ^2) distribution of the excess events for the Crab nebula. R_{68}^2 is denoted by the dashed line. The angular distance is calculated with respect to the position of the Crab pulsar.